Asian Journal of Chemistry; Vol. 38, No. 4 (2026), 886-894
ASIAN JOURNAL OF CHEMISTRY
https://doi.org/10.14233/ajchem.2026.35250

Biogenic Calcium Oxide Nanoparticles: Green Synthesis, Hemocompatibility and Dye Adsorption Studies

A. MALARVIZHI[1], C. STELLA PACKIAM[1,*], M.I. DELIGHTA MANO JOYCE[2], R. GOMATHI[3] and H. KOHILA SUBATHRA CHRISTY[2]

[1]Department of Chemistry, A.P.C. Mahalaxmi College for Women (Affiliated to Manonmaniam Sundaranar University, Tirunelveli), Tuticorin-628002, India
[2]Department of Chemistry, Sadakathullah Appa College, Tirunelveli-627011, India
[3]Department of Chemistry, Sree Devi Kumari Women's College, Kuzhithurai-629163, India

*Corresponding author: E-mail: stellapackiam@apcmcollege.ac.in

Received: 13 November 2025 *Accepted*: 27 January 2026 *Published online*: 8 April 2026 AJC-22309

Calcium oxide (CaO) is a highly efficient chemisorbent and catalyst for the mitigation of hazardous gases, rendering it an important material in industrial and environmental applications. In present study, CaO nanoparticles (CaO NPs) were synthesised using a green hydrothermal approach using the marine squid (*Sepioteuthis lessoniana*) ethanol extract as a natural precursor. XRD analysis confirmed the crystalline nature, with an average crystallite size of 48.12 nm as estimated using the Debye-Scherrer equation. The successful conversion of the marine squid extract into CaO NPs was verified by FTIR and XRD analyses. Transmission electron microscopy (TEM) revealed spherical nanoparticles with an average particle size of approximately 50 nm. Field emission scanning electron microscopy (FESEM) images showed predominantly spherical particles with porous, rough surfaces and aggregation observed at the elevated temperatures. The synthesised CaO NPs demonstrated a high adsorption efficiency toward methyl red (MR) dye, with a maximum adsorption capacity of 42.34 mg/g and a Freundlich constant (K_f) of 22.45 (mg/g)(mg/L)^n. Adsorption data exhibited an excellent fit with the Langmuir and Freundlich isotherm models, while Temkin isotherm and quantum chemical analyses suggested that the adsorption mechanism was predominantly physical in nature.

Keywords: Green synthesis, Calcium oxide nanoparticles, *Sepioteuthis lessoniana*, Methyl red dye, Adsorption isotherms.

INTRODUCTION

Water, the universal solvent, faces severe contamination from dyes, solvents, herbicides, fertilizers, heavy metals and pharmaceuticals, which contribute to a global scarcity of safe drinking water, especially in industrialised areas. Dyes hinder light in aquatic environments, affecting photosynthesis and disrupting ecosystems [1-3]. Methyl red (MR), a synthetic azo dye, is poorly soluble in water but dissolves in organic solvents. It is used as an acid-base indicator and in textiles, yet wastewater containing methyl red poses significant environmental and health risks [4]. Prolonged exposure to methyl red dye can cause skin damage, irritation of the eyes and intestines and is associated with carcinogenic, mutagenic and toxic effects [4]. Its stable aromatic structure and azo groups lead to the generation of harmful aromatic amines.

Calcium oxide nanoparticles (CaO NPs) have gained considerable attention due to their low toxicity and environmentally friendly nature, which makes them highly suitable for environmental remediation and biomedical applications [5,6]. Their significance has further increased with the development of green synthesis approaches that provide a sustainable and cost effective route for producing CaO NPs with minimal environmental impact, making them particularly attractive for wastewater treatment applications [7,8]. The effectiveness of CaO NPs in such processes is mainly attributed to their high surface basicity, strong chemisorption capability and notable catalytic activity, which facilitate efficient gas capture, pollutant adsorption and catalytic reactions [9]. In addition, CaO is naturally abundant, inexpensive, thermally stable and ecologically compatible, further supporting its potential for large-scale industrial and environmental applications [10,11].

Marine extracts are unique compared to plant extracts, comprising marine specific biomolecules (proteins, peptides, amino acids, chitin derived chemicals and minerals) that enhance nanoparticle formation [12]. These biomolecules

improve the surface functionality, stability and bioactivity of nanoparticles which is less common in plant extracts [13,14]. Utilizing squid extract for CaO NPs synthesis offers a sustainable method in the marine biogenic nanotechnology [15]. The biogenic CaO NPs have potential in biomedical applications including cytotoxicity assessments with red blood cells and in environmental uses for the adsorption of harmful dyes like methyl red [16].

Marine-derived proteins and biopolymers may affect the nucleation, size and morphology of CaO NPs differently than plant-based biomolecules. Although CaO NPs have shown strong adsorption performance toward several dyes and comprehensive comparative studies with conventional adsorbents including activated carbon and modified CaO NPs, particularly in the context of marine-mediated synthesis, are still scarce. The present study focuses on the biogenic synthesis of CaO NPs using the ethanol extract of marine squid (*Sepioteuthis lessoniana*) and evaluates their hemolytic activity and adsorption performance for methyl red dye.

EXPERIMENTAL

Preparation of CaO NPs: Fresh marine squid was collected, thoroughly washed with distilled water to remove the impurities and then shade-dried. The dried squid tissue was finely powdered and subjected to extraction using ethanol. Aqueous $CaCl_2$ solution (80 mL of 1 M) was added dropwise while being continuously stirred to 20 mL of *S. lessoniana* extract followed by the addition of NaOH solution and the solution was stirred using a magnetic stirrer. The reaction mixture was maintained at room temperature until the formation of a white precipitate was observed, indicating the formation of CaO NPs. The suspension was centrifuged at 10,000 rpm for 20-30 min and the precipitate was washed several times with distilled water to remove residual biomolecules. The product was dried at 100-125 ºC and calcined at 400 ºC for 2-4 h to convert intermediate calcium compounds into CaO NPs. The obtained CaO NPs were stored in airtight containers for further studies.

Characterisation: The biogenic CaO NPs were characterized using several analytical techniques. The optical properties were examined using a UV-visible spectrophotometer (JASCO V-650) within the wavelength range of 300-700 nm, with double-distilled water used as the reference. Functional groups involved in nanoparticle formation and stabilization were identified through Fourier transform infrared (FTIR) spectroscopy using a Thermo Scientific iS5 instrument in the range of 4000-400 cm^{-1} using KBr pellet method. The crystalline nature of the nanoparticles was investigated by X-ray diffraction (XRD) using an XPERT-PRO diffractometer operated at 30 kV and 30 mA with Cu*K*α radiation (λ = 1.5406 Å) and the crystallite size was estimated using the Debye-Scherrer equation. The hydrodynamic particle size distribution was measured using dynamic light scattering (DLS) on an Anton Paar Litesizer after dispersing the sample in Millipore water. Surface morphology was observed using scanning electron microscopy (SEM) with a Carl Zeiss Ultra Plus FEGSEM operated at 10-30 kV, where the samples were coated with a thin gold layer to improve conductivity. In addition, transmission electron microscopy (TEM) was used to further examine the particle size and morphology by depositing ethanol-dispersed nanoparticles onto carbon-coated copper grids.

Cyclic voltammetry (CV) analysis: The electrochemical measurements were carried out using a CHI 650C electrochemical workstation. In reversible electrochemical systems, the redox couple remains in equilibrium during the potential sweep and the corresponding peak current (I_p) can be determined using the Randles–Sevcík equation, which is expressed as:

$$I_p = (2.69 \times 10^5) n^{3/2} A D^{1/2} C \nu^{1/2}$$

where I_p is the peak current (A); n is the number of electrons transferred; A is the electrode area (cm^2); D is the diffusion coefficient (cm^2/s); C is the concentration of the electroactive species (mol/cm^3); and ν is the scan rate (V/s).

Adsorption study: Batch adsorption studies were conducted to examine the effect of various experimental parameters including temperature, ionic strength, adsorbent dosage, contact time and pH, on the removal of methyl red (MR) dye using the synthesized CaO NPs. In each set of experiments, one parameter was varied while the remaining conditions were kept constant to evaluate its individual influence on the adsorption process. For example, during the investigation of contact time, only the duration of interaction was altered, whereas temperature, pH and adsorbent dosage were maintained at fixed values.

The equilibrium adsorption capacity (Q_e) of methyl dye on CaO NPs was calculated using the following equation:

$$Q_e\,(mg/g) = \frac{C_i - C_e}{1} \times \frac{v}{m}$$

where Q_e (mg/g) is the amount of dye adsorbed at equilibrium, C_i (mg/L) is the initial concentration of methyl red dye solution, C_e (mg/L) is the equilibrium concentration, V (L) is the volume of dye solution and m (g) is the mass of adsorbent.

The percentage removal of methyl red dye was determined using the following relation:

$$\text{Removal}\,(\%) = \frac{C_i - C_e}{C_i} \times 100$$

The measurements of the residual methyl red dye concentration were performed at the maximum absorbance wavelength (λ_{max}) of 525 nm using a UV-Visible spectrophotometer.

Hemolysis assay: Blood compatibility was determined through a hemolysis assay. Initially, 2 mL of blood was diluted with 4 mL of Dulbecco's phosphate-buffered saline (D-PBS) and centrifuged at 10,000 g for 5 min to separate red blood cells (RBCs). The collected RBCs were washed five times with 10 mL D-PBS to remove plasma residues and then resuspended to a final volume of 20 mL with D-PBS. For the assay, 0.2 mL of diluted RBC suspension was mixed with 0.8 mL of nanoparticle suspension prepared in D-PBS to obtain final concentrations of 5, 10, 25, 50 and 100 µg/mL. Distilled water and D-PBS were used as positive and negative controls, respectively, and each condition was tested in quadruplicate. The mixtures were incubated at room temperature for 4 h, followed by centrifugation for 5 min and then 100 µL of the

supernatant from each sample was transferred into a 96-well plate and absorbance was measured at 577 nm using a microplate reader (TECAN Infinite M200, Austria) with 655 nm as the reference wavelength. The haemolytic degree was expressed by the hemolytic ratio as the following formula:

$$\text{Hemolysis ratio (\%)} = \frac{OD_{test} - OD_{negative\ control}}{OD_{positive\ control} - OD_{negative\ control}} \times 100$$

The CaO NPs synthesized using squid extract exhibited good blood compatibility and were classified as non-hemolytic, showing less than 1% hemolysis up to a concentration of 100 μg/mL. At relatively higher concentrations of 50 and 100 μg/mL, hemolysis ratios of 0.771% and 0.784%, respectively, were observed. These results indicate that even at higher concentrations, the CaO NPs induce only minimal hemolytic effects on red blood cells. The slight increase in hemolysis at higher nanoparticle concentrations may be associated with mild oxidative stress generated during the interaction of CaO NPs with blood cells [17].

RESULTS AND DISCUSSION

UV-Visible spectroscopy: Fig. 1 displays the UV-visible absorption spectrum of biogenic CaO NPs reveals distinct bands at 255, 290 and 345 nm, primarily linked to electronic transitions rather than surface proteins. The band at 255 nm corresponds to charge-transfer transitions between O^{2-} (2p) and Ca^{2+} states, typical in CaO and other alkaline earth metal oxides. These nanoparticles show deep-UV absorption bands due to their broad band-gap of approximately 7.0 eV [18,19]. The peak at 290 nm in CaO NPs is attributed to defect-related states and surface oxygen vacancies, commonly observed due to lattice defects and surface hydroxylation. Furthermore, a broader absorption characteristic near 345 nm is associated with surface states and electronic transitions influenced by particle size. Smaller nanoparticles exhibit red shifts and band tailing, extending absorption into the near-UV range [20].

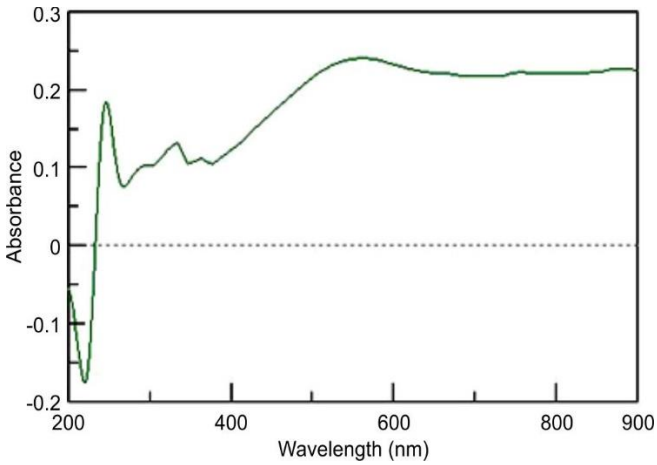

Fig. 1. Absorbance spectrum of CaO NPs synthesised with *S. lessoniana*

The band gap energy (E_{BG}) of the biogenic CaO NPs was estimated from the wavelength of maximum absorption λ_{max} using Planck's relation ($E_{BG} = hc/\lambda_{max}$), where 'h' represents Planck's constant and 'c' is the speed of light. The calculated band gap value was 4.86 eV, which is consistent with previously reported values for CaO NPs applied in photocatalytic systems (around 4.0-4.8 eV) [21]. Nevertheless, this value is higher than the commonly reported band gap range of 2.61-3.65 eV [22], possibly due to the variations in nanoparticle size, synthesis conditions or surface properties.

The UV-Vis absorption behaviour of the synthesized CaO NPs is linked to the interaction between Ca^{2+} ions and bioactive compounds present in the squid extract, which function as reducing, capping and stabilizing agents during the green synthesis process. The pronounced absorption in the deep UV region can be attributed mainly to $\pi \rightarrow \pi^*$ and $n \rightarrow \pi^*$ electronic transitions associated with aromatic amino acids, peptides and other organic molecules in the extract. In addition, ligand-to-metal charge transfer between Ca^{2+} ions and functional groups of these biomolecules may contribute to the observed spectral features. The presence of such biomolecules on the nanoparticle surface helps inhibit particle aggregation and improves stability.

FTIR spectral studies: In the IR spectrum of biogenic CaO NPs (Fig. 2), a broad and intense absorption band at 3456 cm^{-1} corresponds to O–H stretching vibrations, indicating the presence of hydroxyl groups and surface-adsorbed water molecules. A band near 1489 cm^{-1} is associated with C–H bending and C=O/C–N vibrations, characteristic of amide-II or carboxylate groups originating from proteins, peptides and other organic compounds present in the squid extract. Although the typical amide-I band (~1650 cm^{-1}) is not clearly observed, the presence of the 1489 cm^{-1} band along with the broad O–H absorption suggests that biomolecules from the extract act as reducing and stabilizing agents on the nanoparticle surface. Furthermore, absorption bands observed around 871 $cm^{-1}$and in the 648-609 cm^{-1} region correspond to the Ca–O stretching vibrations, confirming the formation of CaO NPs and the presence of metal–oxygen bonds within their crystalline structure.

XRD studies: The obtained diffraction peaks closely match those of standard CaO (JCPDS card No. 37-1497), confirming the formation of pure CaO with a cubic phase. The multiple characteristic diffraction peaks at 2θ values of 32º, 37º, 48º, 53º, 64º, 69º and 77º, corresponding to the lattice planes (111), (200), (211), (220), (311), (222) and (400), respectively. These reflections are indexed to a cubic crystal system with a lattice parameter of α = 4.8152 Å, assigned to the $Fm\bar{3}m$ space group [23,24]. The average crystallite size (D) was calculated using the Debye–Scherrer equation:

$$D = \frac{K\lambda}{\beta \cos\theta}$$

where K is the shape factor (0.9), λ is the X-ray wavelength (1.54 Å), λ is the full width at half maximum (FWHM) and θ is the Bragg diffraction angle. The average crystallite size of the biogenic CaO NPs was found to be approximately 48.12 nm, while the most intense diffraction peak observed at 2θ = 29º corresponded to a smaller crystalline size of 9.65 nm (Fig. 3). The predominant diffraction peak at 2θ = 32º agrees well with previously reported values for CaO NPs [25], confirming that the synthesised CaO NPs possess a cubic monophasic structure with excellent crystallinity [26].

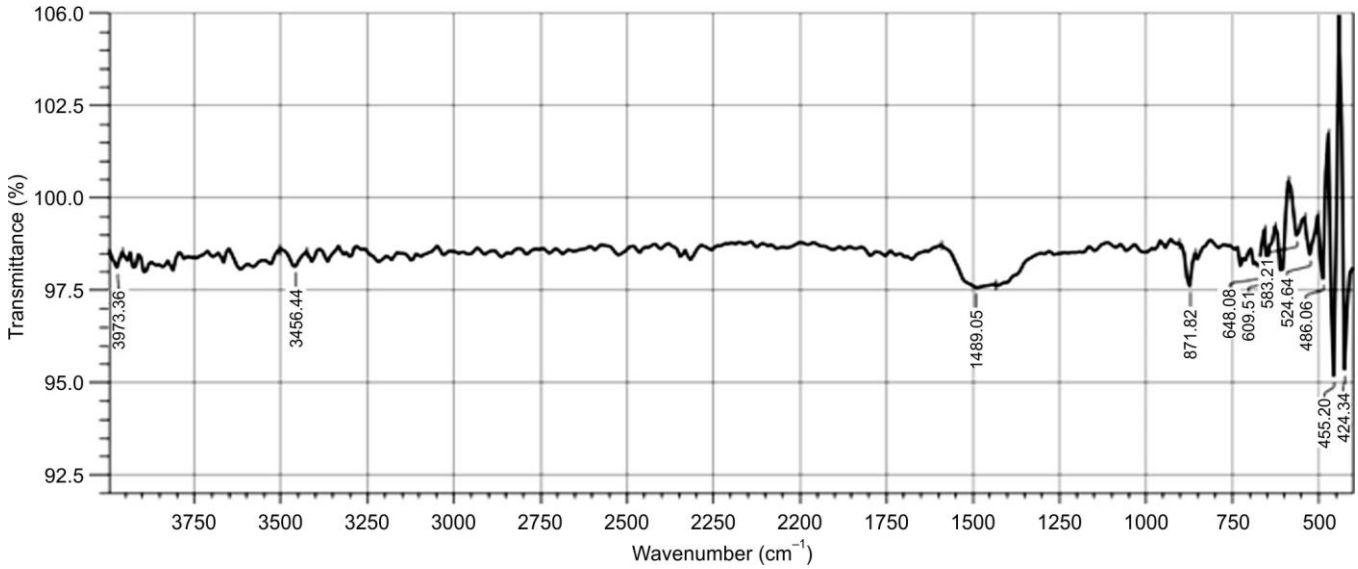

Fig. 2. FTIR spectrum of CaO NPs synthesised with *S. lessoniana*

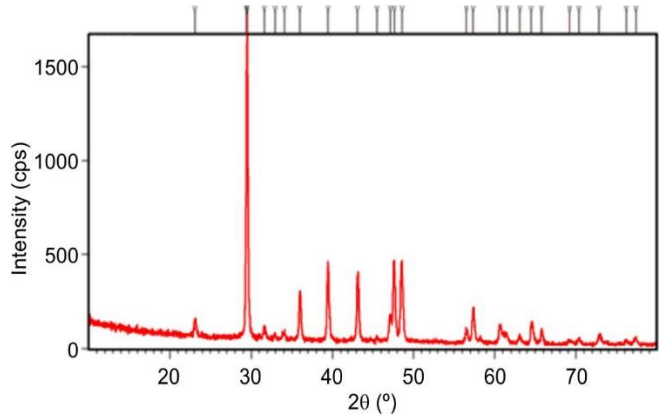

Fig. 3. XRD studies of CaO NPs synthesised with *S. lessoniana* extract

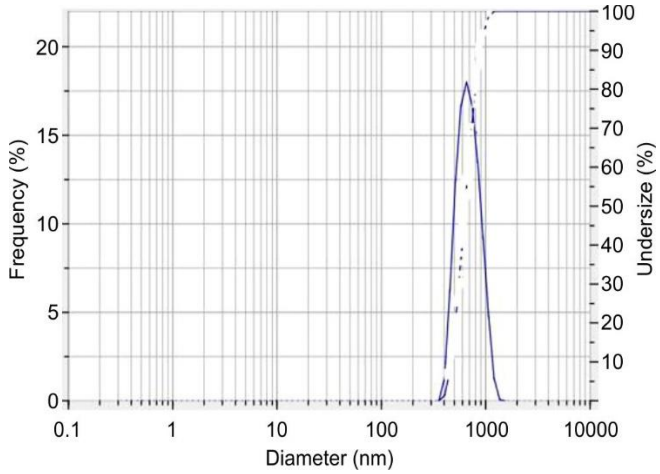

Fig. 4. DLS analysis of CaO NPs synthesised with *S. lessoniana* extract

DLS analysis: DLS analysis of the biogenic CaO NPs revealed a Z-average hydrodynamic diameter of 1097.2 nm with a polydispersity index (PDI) of 1.117, indicating a broad and highly heterogeneous size distribution dominated by large aggregates (Fig. 4). In contrast, TEM images showed primary nanoparticles in the range of 15-30 nm, suggesting that these smaller particles tend to aggregate in aqueous media to form larger clusters, a common phenomenon in green-synthesized nanoparticles due to intermolecular interactions and biomolecular capping. Despite this aggregation, FESEM and TEM observations indicated rough and porous surface morphologies, which provide abundant active sites and facilitate dye adsorption through accessible exterior surfaces and pore networks [27,28]. Thus, the adsorption efficiency remains largely unaffected by aggregation. However, the relatively large hydrodynamic size and high polydispersity may restrict certain biomedical applications, particularly intravenous use. Although the nanoparticles exhibit acceptable hemocompatibility, further surface modification or size stabilization would be beneficial to enhance their suitability for advanced biological applications [29,30].

SEM studies: The surface morphology of the biogenic CaO NPs was examined using scanning electron microscopy (SEM) at a magnification of 10.00 KX with scale bars of 2 μm and 10 μm. The SEM images (Fig. 5) reveal a heterogeneous morphology consisting of rounded and irregularly shaped particles that tend to assemble into aggregated clusters rather than remaining individually dispersed. These clusters form porous, network-like structures composed of numerous smaller particles that merge into larger agglomerates ranging from approximately 1-5 μm, while the primary particles are in the nanometer range. Such aggregation behaviour is commonly observed in biogenic nanoparticles, where the biomolecules present in the marine squid extract act as reducing, stabilizing and capping agents during nanoparticle formation. The rough surface texture and irregular morphology further indicate the presence of organic residues associated with bio-capping on the nanoparticle surface. In addition, a dense, rock-like particle distribution suggests partial fusion of smaller particles during the drying and calcination stages. The relatively larger particle size compared with materials synthesized under lower calcination temperatures is consistent with UV-Vis results, which indicate a decrease in band gap with increasing particle size at higher temperatures [31]. Although CaO NPs exhibit a tendency

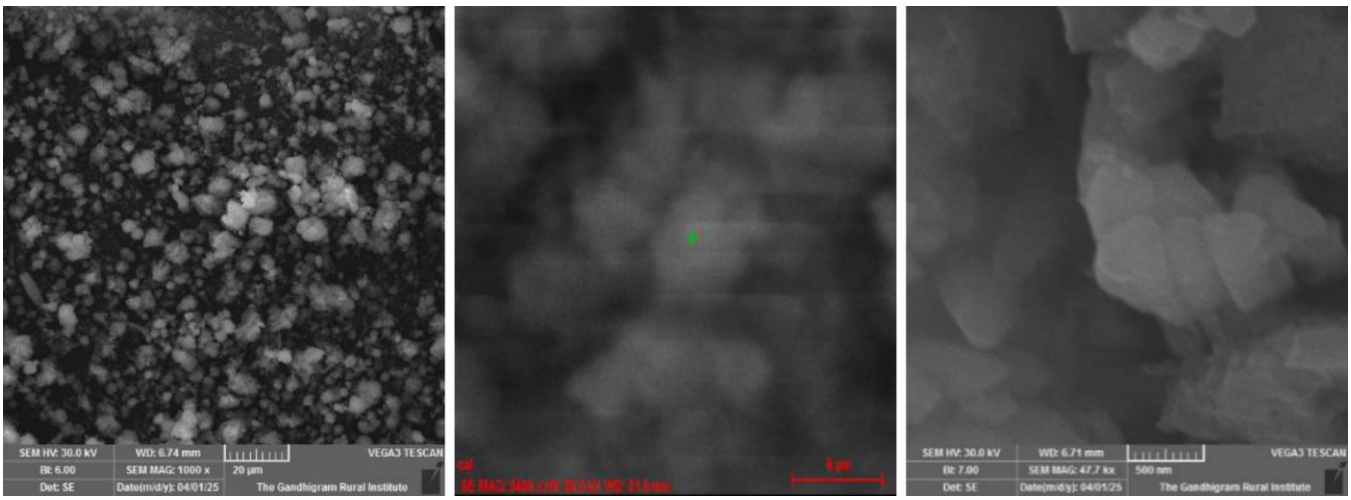

Fig. 5. SEM studies of CaO NPs synthesised with *S. lessoniana* extract

to agglomerate due to high surface energy, electrostatic interactions and surface reactions with atmospheric moisture and CO_2, this aggregation does not negatively affect their adsorption performance. Instead, the resulting rough and porous agglomerates provide accessible active sites for dye adsorption and facilitate easier separation from aqueous systems, making them particularly suitable for environmental and catalytic applications [27-30].

TEM studies: The TEM micrographs, obtained at magnifications within the 5-200 nm scale range, show nanosized particles with predominantly spherical to irregular morphologies (Fig. 6). The particle size was mainly distributed between 10 and 50 nm, with an average grain size of approximately 55 nm, which is slightly larger than the crystallite size estimated from XRD due to the difference in measurement principles, as TEM reflects the actual particle size including aggregation effects whereas XRD represents the coherent crystallite domains. The selected area electron diffraction (SAED) pattern displays clear concentric rings corresponding to the (111), (200), (220) and (311) lattice planes, confirming the polycrystalline nature and face-centered cubic (FCC) structure of CaO, consistent with the standard JCPDS card No. 37-1497. The presence of well-defined diffraction rings indicates good crystallinity of the synthesized nanoparticles. The TEM observations, together with SEM and XRD analyses, confirm the successful formation of crystalline CaO NPs with nanoscale dimensions, which are suitable for applications such as adsorption and catalysis [32,33].

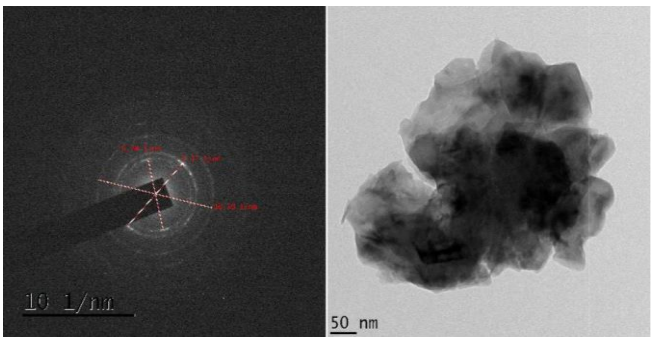

Fig. 6. TEM studies of CaO NPs synthesised with *S. lessoniana* extract

EDAX studies: The EDAX spectrum of the biogenic CaO NPs (Fig. 7) confirms the presence of calcium (Ca), oxygen (O) and minor traces of phosphorus (P) and potassium (K), with prominent peaks appearing around 0.3 keV, 2.0 keV and 3.7 keV, respectively. The strong signals for Ca and O indicate that the NPs are predominantly composed of calcium oxide, while the minor elements likely originate from biomolecules present in the marine squid extract used during synthesis. Thus, the EDAX analysis supports the XRD and FTIR findings, confirming the successful formation, high purity and elemental stability of the biogenic CaO NPs.

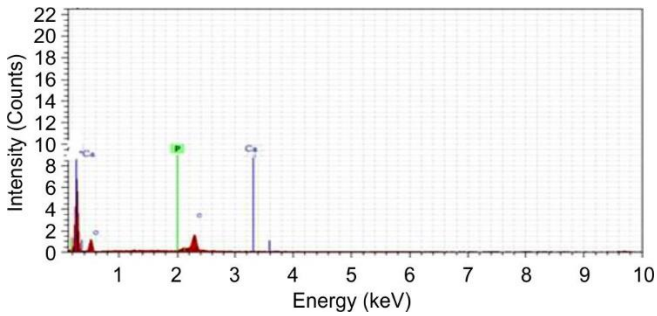

Fig. 7. EDAX studies of CaO NPs synthesised with *S. lessoniana* extract

CV analysis: Cyclic voltammetry (CV) was performed to assess the electrochemical behaviour of biogenic CaO NPs using an electrolyte of 1 M KOH within a potential range of 0.001-0.1 V *vs.* Ag/AgCl. The CV curves (Fig. 8), recorded at scan rates between 0.025 and 0.1 mV s^{-1}, revealed distinct cathodic and anodic peaks at approximately 0.37 V and -0.43 V, respectively, confirming the reversible redox nature of the system. The nearly symmetrical CV profiles with increasing scan rates indicate stable electron transfer kinetics and strong electrochemical reversibility. The enhanced electrocatalytic activity and charge storage capacity are attributed to bioactive compounds present in the marine squid extract, which act as natural stabilizers and capping agents, improving electron transport and ion diffusion at the electrode–electrolyte interface, which is crucial for excellent capacitive and redox properties for applications in the electrochemical sensors, energy storage systems and biomedical devices.

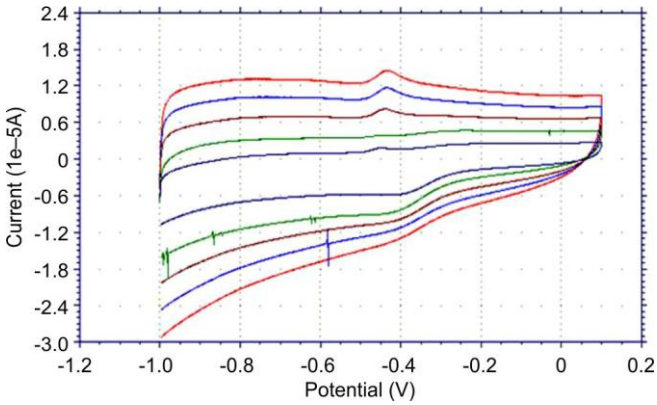

Fig. 8. CV studies of CaO NPs synthesised with *S. lessoniana* extract

Adsorption studies: Adsorption studies were conducted to evaluate the efficiency of biogenic CaO NPs in removing methyl red dye from aqueous solutions through batch adsorption experiments. The effects of key parameters such as contact time (10-60 min), adsorbent dosage (20-120 mg), dye concentration (10-35 mg/L) and pH (2-12) were systematically examined to determine their influence on dye removal efficiency. The methyl red dye concentration was monitored at its maximum absorption wavelength of 570 nm. As shown in Fig. 9a, the adsorption of methyl red dye increased with stirring time, exhibiting a rapid uptake during the initial 10 min, where nearly 30% of the dye was removed within the first 30 min. Beyond this point, the adsorption rate slowed, suggesting that equilibrium was achieved due to saturation of the active adsorption sites on the CaO NPs. These results indicate that the biogenic CaO NPs effectively adsorb methyl red dye, with the process primarily governed by the availability of active surface sites and contact duration [34].

The equilibrium adsorption of methyl red dye increased with rising initial dye concentration (Fig. 9b). Higher concentrations provide a greater number of dye molecules in solution, which enhances their interaction with the available adsorption sites on the surface of CaO NPs. Comparable trends have been reported for dye adsorption using CaO-based materials, where adsorption capacity increases with concentration until the active sites become saturated [35]. In this study, saturation was not reached within the tested concentration range indicating that the adsorption capacity of the biogenic CaO NPs may continue to increase at higher dye concentrations.

The influence of adsorbent dosage was evaluated by varying the amount of CaO NPs from 20 to 120 mg in 50 mL of methyl red dye solution with a stirring time of 30 min. As illustrated in Fig. 9c, dye removal efficiency improved with increasing adsorbent dosage and reached a maximum removal efficiency of 97% at 120 mg. This improvement can be associated with the greater surface area and higher number of active adsorption sites available for dye interaction. However, excessive adsorbent loading may promote particle aggregation or overlap of adsorption sites, which can slightly reduce the effective surface area accessible for adsorption [36].

The effect of solution pH on methyl red dye adsorption was investigated within the pH range of 2-12 (Fig. 9d). The adsorption efficiency increased under acidic conditions and reached a maximum removal of 93% at pH 6, followed by a decline to about 53% at pH 8, with a slight increase again under alkaline conditions. These variations are mainly related to changes in the surface charge of the adsorbent and the electrostatic interactions between the dye molecules and the nanoparticle surface. Under acidic conditions, the CaO NPs surface acquires a positive charge, which enhances the attraction toward negatively charged dye species. As the pH approaches neutral or alkaline values, repulsive interactions become more significant, leading to lower adsorption efficiency. Similar pH-dependent behaviour has been observed in earlier studies on methyl dye adsorption [37].

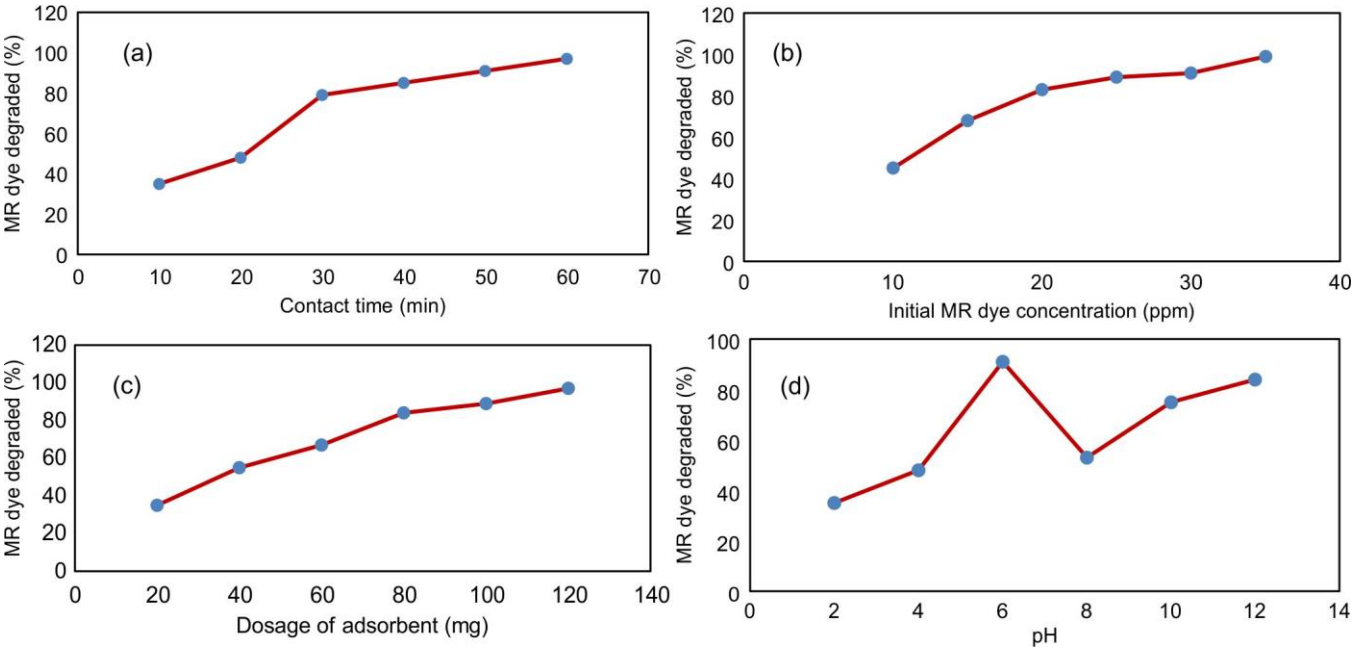

Fig. 9. Percentage adsorption studies of methyl red dye using CaO NPs under varying conditions: (a) effect of contact time, (b) effect of initial dye concentration, (c) effect of adsorbent dosage and (d) effect of pH

FTIR interpretation for adsorption studies: FTIR analysis was conducted to identify the functional groups in the adsorption of MR dye onto CaO NPs derived from marine squid extract. It was found that revealed that CaO NPs prior to adsorption show a broad absorption band at 3600-3400 cm^{-1} indicating O–H stretching of hydroxyl groups and moisture, with a faint band at 1500-1450 cm^{-1} related to carbonate species (Fig. 10). The MR dye spectrum highlights N–H stretching at ~3400 cm^{-1}, aromatic C=C stretching at 1600-1650 cm^{-1} and peaks around 1500-1400 cm^{-1} for azo and C–N vibrations. Post-adsorption, the CaO NPs display a diminished O–H band suggesting hydrogen bonding with the dye, with confirmed adsorption through changes in characteristic MR peaks and minor alterations in the Ca-O vibration band below 600 cm^{-1} indicating interactions with CaO lattice sites.

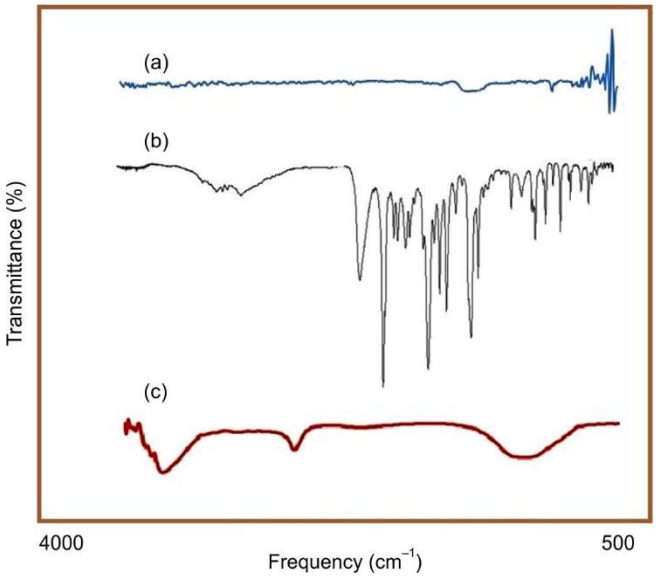

Fig. 10. FTIR spectra of (a) squid extract (*S. lessoniana*), (b) methyl red dye and (c) methyl red dye after interaction with biogenic CaO NPs

Adsorption isotherms: The adsorption isotherm for the removal of methyl red dye by biogenic CaO NPs was analysed using the Langmuir, Freundlich and Temkin models to understand the interaction between the adsorbate and adsorbent surfaces (Fig. 11a-c). The Langmuir isotherm indicated a maximum monolayer adsorption capacity (Q_e) of 42.34 mg/g, with an adsorption intensity factor ($R_L < 1$) confirming the favourability of the process and a correlation coefficient (R^2) of 0.6593. The Freundlich isotherm also showed a strong correlation ($R^2 = 0.6624$), with a Freundlich constant (K_F) of 22.45 $(mg/g)(mg/L)^n$ and an exponent ($1/n = 0.3928$), suggesting a heterogeneous surface and multilayer adsorption. The lower reduced chi-square value obtained for the Freundlich model compared to the Langmuir model indicates a better fit, implying that the adsorption process is likely heterogeneous in nature. The Temkin isotherm was also evaluated, where the constants B_T (J/mol) and A_T (L/mg) were determined from the slope and intercept of the plot of Q_e *versus* ln C_e, providing information on the binding energy and heat of adsorption. The results (Table-1) indicate that the Freundlich model provides the best fit for the adsorption of methyl red dye onto

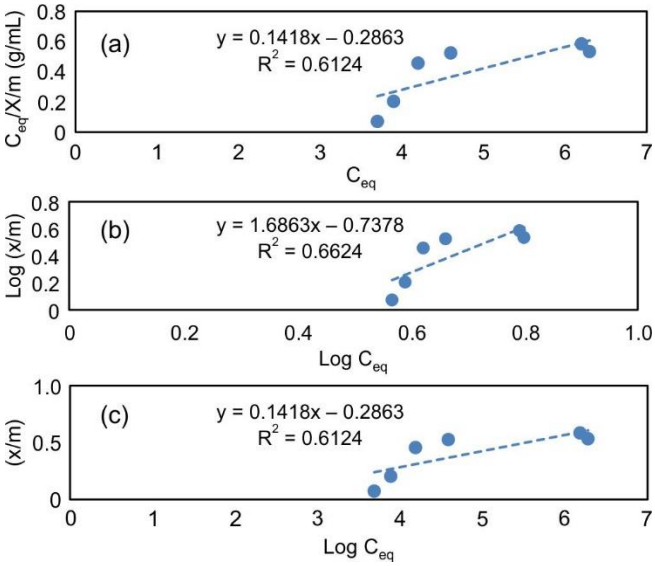

Fig. 11. Plots of (a) Langmuir isotherm, (b) Freundlich isotherm and (c) Temkin isotherm for MR dye adsorption onto CaO NPs using marine squid extract at pH 6, a contact time of 60 min, an adsorbent dosage of 100 mg/50 mL and a temperature of 30 ºC

TABLE-1
ADSORPTION ISOTHERM PARAMETERS DATA OF CaO NPs TOWARDS METHYL RED DYE

Model	Parameter	Value
Langmuir	Q_{max} (mg/g)	42.34
	R_L	< 1
	R^2	0.6363
Freundlich	KF $(mg/g)(mg/L)^n$	22.45
	1/n	0.3928
	R^2	0.6624
Temkin	B_T (J/mol)	0.1416 (from slope)
	A (L/g)	-0.2863
	R^2	~0.636

CaO NPs, suggesting multilayer adsorption on a heterogeneous surface influenced by bioactive compounds present in the squid extract [38,39].

Adsorption mechanism: In this study, the point of zero charge (pH_{pzc}) was determined to be 6, indicating that the adsorbent surface is electrically neutral at this pH. When the solution pH is below the pH_{pzc}, the surface becomes positively charged, whereas at pH values above the pH_{pzc} the surface acquires a negative charge. The maximum adsorption of methyl red dye was observed at pH 6, suggesting that adsorption is favoured under near-neutral conditions. Variations in adsorption efficiency at different pH values are primarily governed by changes in surface charge and the resulting electrostatic interactions between the dye molecules and the adsorbent surface.

Hemolysis assay: The hemolytic behaviour of *S. lessoniana* mediated CaO NPs was evaluated by incubating them with red blood cells at different concentrations. At 5 µg/mL, the nanoparticles exhibited a hemolysis ratio of 0.591%, indicating negligible damage to erythrocytes. With increasing concentrations of 10, 25, 50 and 100 µg/mL, the hemolysis

ratios gradually increased to 0.617%, 0.683%, 0.715% and 0.773%, respectively (Table-2). This slight increase at higher concentrations may result from interactions between the CaO NPs and red blood cell membranes that can induce mild oxidative stress [40-42]. However, the hemolysis values for all tested concentrations remained below 1%, which is well under the ASTM F756 non-hemolytic threshold of 2%, confirming the good hemocompatibility of the biogenic CaO NPs and their suitability for potential biomedical applications.

TABLE-2
HEMOLYTIC ASSAY DATA OF
CaO NPs USING *Sepioteuthis lessoniana*

Concentration (µg/mL)	Hemolysis (%)
5	0.591
10	0.617
25	0.683
50	0.715
100	0.773

Conclusion

This study reports that calcium oxide nanoparticles (CaO NPs) can be effectively synthesised through a green hydrothermal process utilizing ethanol extract of marine squid (*Sepioteuthis lessoniana*), providing a cost-effective alternative to conventional chemical methods. The marine biomolecules significantly influence nanoparticle morphology and surface functionalisation, enhancing the structural and surface qualities of the biogenic CaO NPs. The biogenic CaO NPs exhibit excellent adsorption capabilities for methyl red dye, making them efficient adsorbents for wastewater treatment, with mechanisms driven by surface interactions and pH-specific charge distribution.

ACKNOWLEDGEMENTS

The authors sincerely acknowledge the Heads of the Departments of Chemistry of their respective institutions for providing access to the laboratory facilities used in this study.

CONFLICT OF INTEREST

The authors declare that there is no conflict of interests regarding the publication of this article.

DECLARATION OF AI-ASSISTED TECHNOLOGIES

During the preparation of this manuscript, the authors used an AI-assisted tool(s) to improve the language. The authors reviewed and edited the content and take full responsibility for the published work.

REFERENCES

1. S. Dutta, S. Adhikary, S. Bhattacharya, S. Chatterjee, A. Chakraborty, D. Roy, D. Banerjee, A. Ganguly, S. Nanda and P. Rajak, *J. Environ. Manag.*, **353**, 120103 (2024); https://doi.org/10.1016/j.jenvman.2024.120103
2. M. Salehi, *Environ. Int.*, **158**, 106936 (2022); https://doi.org/10.1016/j.envint.2021.106936
3. M. Kumar, V. P. Singh, S. B. Bhat and R. Kumar, *Discov. Environ.*, **3**, 132 (2025); https://doi.org/10.1007/s44274-025-00337-0
4. M.D. Teweldebrihan and M.O. Dinka, *Water*, **16**, 2237 (2024); https://doi.org/10.3390/w16162237
5. R.J. Griffitt, J. Luo, J. Gao, J.C. Bonzongo and D.S. Barber, *Environ. Toxicol. Chem.*, **27**, 1972 (2008); https://doi.org/10.1897/08-002.1
6. A. Rana, K. Yadav and S. Jagadevan, *J. Clean. Prod.*, **272**, 122880 (2020); https://doi.org/10.1016/j.jclepro.2020.122880
7. K.K. Jaiswal, S. Dutta, C.B. Pohrmen, R. Verma, A. Kumar and A.P. Ramaswamy, *Inorg. Nano-Met. Chem.*, **51**, 995 (2021); https://doi.org/10.1080/24701556.2020.1813769
8. Sanjana, R. Priyadharshini, S. Rajeshkumar and J. Anandan, *J. Environ. Nanotechnol.*, **14**, 63 (2025); https://doi.org/10.13074/jent.2025.03.243941
9. A. Samanta, A. Zhao, G.K.H. Shimizu and P. Sarkar, *Ind. Eng. Chem. Res.*, **51**, 1438 (2012); https://doi.org/10.1021/ie200686q
10. W. Liu, H. An, C. Qin, J. Yin, G. Wang, B. Feng and M. Xu, *Energy Fuels*, **26**, 1190 (2012); https://pubs.acs.org/doi/10.1021/ef300220x
11. C. Shen, G. Wu, J. Sun, J. Hou, H. Sun, K. Ding, W. Liu and S. Zhang, *J. Environ. Chem. Eng.*, **11**, 109616 (2023); https://doi.org/10.1016/j.jece.2023.109616
12. S.K. Kim and E. Mendis, *Food Res. Int.*, **39**, 383 (2006); https://doi.org/10.1016/j.foodres.2005.10.010.
13. N. Ramaraj, G. Thiripuranathar, S. Ekanayake, K. Attanayake and U. Marapana, *RSC Sustain.*, **3**, 2567 (2025); https://doi.org/10.1039/D5SU00014A
14. J.K. Tee, C.N. Ong, B.H. Bay, H.K. Ho and D.T. Leong, *Wiley Interdiscip. Rev. Nanomed. Nanobiotechnol.*, **8**, 414 (2016); https://doi.org/10.1002/wnan.1374
15. D.Y. Pujiastuti, M.N. Ghoyatul Amin, M.A. Alamsjah and J.-L. Hsu, *Molecules*, **24**, 2541 (2019); https://doi.org/10.3390/molecules24142541
16. C.S. Packiam, A. Malarvizhi, H.K.S. Christy, A. Dhivya and M. Paripooranaselvi, *Cur. Trends Pharm. Pharma Chem.*, **7**, 73 (2025); https://doi.org/10.18231/j.ctppc.2025.012
17. L.Y. Wang and L.K. Kaczmarek, *Nature*, **394**, 384 (1998); https://doi.org/10.1038/28645
18. J.P. Singh, W.C. Lim, S.O. Won, J. Song and K.H. Chae, *J. Korean Phys. Soc.*, **72**, 890 (2018); https://doi.org/10.3938/jkps.72.890
19. F. Zhang, D. Pant and B.E. Logan, *Biosens. Bioelectron.*, **30**, 49 (2011); https://doi.org/10.1016/j.bios.2011.08.025.
20. U.U. Khan, K. Rehman, K. Gul, S. Munir and Z.A. Sha, *Prog. Chem. Biochem. Res.*, **9**, 130 (2026); https://doi.org/10.48309/pcbr.2026.543134.1462
21. N.O. Eddy, J. Oladede, I.S. Eze, R. Garg, R. Garg and H. Paktin, *Results Eng.*, **24**, 103374 (2024); https://doi.org/10.1016/j.rineng.2024.103374
22. T. Qu, X. Yao, G. Owens, L. Gao and H. Zhang, *Sci. Rep.*, **12**, 2988 (2022); https://doi.org/10.1038/s41598-022-06981-3
23. T.Í.S. Oliveira, M.F. Rosa, F.L. Cavalcante, P.H.F. Pereira, G.K. Moates, N. Wellner, S.E. Mazzetto, K.W. Waldron and H.M.C. Azeredo, *Food Chem.*, **198**, 113 (2016); https://doi.org/10.1016/j.foodchem.2015.08.080
24. H.K. Chahal, S. Matthews and M.I. Jones, *J. Therm. Spray Technol.*, **32**, 1465 (2023); https://doi.org/10.1007/s11666-023-01582-6
25. S.S. Tabrizi Hafez Moghaddas, S. Samareh Moosavi and R. Kazemi Oskuee, *Biomass Convers. Biorefin.*, **14**, 5125 (2024); https://doi.org/10.1007/s13399-022-02643-6
26. N. Gandhi, Y. Shruthi, G. Sirisha and C.R. Anusha, *Haya Saudi J. Life Sci.*., **6**, 89 (2021).
27. K.Y. Foo and B.H. Hameed, *Chem. Eng. J.*, **156**, 2 (2010); https://doi.org/10.1016/j.cej.2009.09.013
28. M. Danaei, M. Dehghankhold, S. Ataei, F.H. Davarani, R. Javanmard, A. Dokhani, S. Khorasani and M.R. Mozafari, *Pharmaceutics*, **10**, 57 (2018); https://doi.org/10.3390/pharmaceutics10020057

29. S. Wang and Y. Peng, *Chem. Eng. J.*, **156**, 11 (2010); https://doi.org/10.1016/j.cej.2009.10.029
30. D. Shrestha, S. Maensiri, U. Wongpratat, S.W. Lee and A.R. Nyachhyon, *J. Environ. Chem. Eng.*, **7**, 103227 (2019); https://doi.org/10.1016/j.jece.2019.103227
31. M.U. Obot, D.S. Yawas and S.Y. Aku, *J. King Saud Univ. Eng. Sci.*, **29**, 284 (2017); https://doi.org/10.1016/j.jksues.2015.10.008
32. Y. Zhang, Y. Chen, P. Westerhoff, K. Hristovski and J.C. Crittenden, *Water Res.*, **42**, 2204 (2008); https://doi.org/10.1016/j.watres.2007.11.036
33. S. Abraham and V.P. Sarathy, *Int. J. Pharm. Sci. Rev. Res.*, **49**, 121 (2018).
34. M.-H. Baek, C.O. Ijagbemi, O. Se-Jin and D.-S. Kim, *J. Hazard. Mater.*, **176**, 820 (2010); https://doi.org/10.1016/j.jhazmat.2009.11.110
35. F.S. Nworie, F.I. Nwabue, W. Oti, E. Mbam and B.U. Nwali, *J. Chil. Chem. Soc.*, **64**, 4365 (2019); https://doi.org/10.4067/s0717-97072019000104365
36. D. Pathania, S. Sharma and P. Singh, *Arab. J. Chem.*, **10**, S1445 (2017); https://doi.org/10.1016/j.arabjc.2013.04.021
37. R.R. Elmorsi, S.T. El-Wakeel, W.A. Shehab El-Dein, H.R. Lotfy, W.E. Rashwan, M. Nagah, S.A. Shaaban, S.A. Sayed Ahmed, I.Y. El-Sherif and K.S. Abou-El-Sherbini, *Sci. Rep.*, **9**, 3356 (2019); https://doi.org/10.1038/s41598-019-39945-1
38. M.A. Ahmad, N. Ahmad and O.S. Bello, *Appl. Water Sci.*, **5**, 407 (2015); https://doi.org/10.1007/s13201-014-0208-4
39. C.K. Enenebeaku, N.J. Okorocha, U.E. Enenebeaku and I.C. Ukaga, *Int. Lett. Chem. Phys. Astron.*, **72**, 52 (2017); https://doi.org/10.56431/p-02ri34
40. Y. Han, X. Wang, H. Dai and S. Li, *ACS Appl. Mater. Interfaces*, **4**, 4616 (2012); https://doi.org/10.1021/am300992x
41. L. Jiang, Y. Yu, Y. Li, Y. Yu, J. Duan, Y. Zou, Q. Li and Z. Sun, *Nanoscale Res. Lett.*, **11**, 57 (2016); https://doi.org/10.1186/s11671-016-1280-5
42. L.Q. Chen, L. Fang, J. Ling, C.Z. Ding, B. Kang and C.Z. Huang, *Chem. Res. Toxicol.*, **28**, 501 (2015); https://doi.org/10.1021/tx500479m